Acta Cryst. (1997). B53, 429–439

Zeolite Rho Loaded with Methylamines. I. Monomethylamine Loadings

CLAUDIA WEIDENTHALER,[a] REINHARD X. FISCHER,[a]* LLOYD ABRAMS[b] AND ALAN HEWAT[c]

[a]*Fachbereich Geowissenschaften der Universität,† Klagenfurter Strasse, D-28359 Bremen, Germany,* [b]*Central Research and Development Department,‡ EI du Pont de Nemours & Co., Experimental Station, Wilmington, DE 19880, USA, and* [c]*Institut Laue–Langevin, F-38042 Grenoble CEDEX 9, France. E-mail: rfischer@min.uni-bremen.de*

(*Received 31 May 1996; accepted 1 October 1996*)

Abstract

Samples of two differently prepared zeolite rho loaded with different amounts of monomethylamine (MMA) were studied in their hydrated and dehydrated forms by X-ray and neutron diffraction. Both zeolites are partially dealuminated, as indicated by nonframework alumina, which is assumed to be Al_2O_3 or AlOOH. Series I was prepared from dry-calcined NH_4-rho at 873 K, series II from steam-calcined NH_4-rho at 773 K. The samples were loaded with different amounts of deuterated MMA, Rietveld refinements yielded the following results for series I (dry): (1) $H_{3.8}$(H-MMA)$_5Cs_{0.2}Al_9Si_{39}O_{96}.Al_2O_3.28H_2O$, X-ray data collection at room temperature, $Im\bar{3}m$, a = 14.9991 (2) Å, R_{wp} = 0.095; (2) composition as in (1), anhydrous and deuterated, neutron data collected at 5 K, disproportionation into two phases in $I\bar{4}3m$, with a = 14.8410 (7) and 14.5273 (11) Å, R_{wp} = 0.038; (3) (H-MMA)$_{8.8}Cs_{0.2}Al_9Si_{39}O_{96}.Al_2O_3.25H_2O$, X-ray data collection at room temperature, $I\bar{4}3m$, a = 14.9771 (2) Å, R_{wp} = 0.090. Series II (steam): (4) $H_{0.3}$(H-MMA)$_5Cs_{0.7}Al_6Si_{42}O_{96}.2.5Al_2O_3.23H_2O$, X-ray data collected at room temperature, $Im\bar{3}m$, a = 15.0323 (2) Å, R_{wp} = 0.124; (5) composition as in (4), anhydrous and deuterated, neutron data collected at 5 K, disproportionation into two phases in $I\bar{4}3m$ with a = 14.9151 (2) and 14.6475 (8) Å, R_{wp} = 0.031. In the hydrated samples MMA resides on the center axis in the α-cage with the N atoms pointing to the single eight-ring; upon dehydration it migrates into the double eight-rings.

1. Introduction

Zeolite rho has been studied extensively since it was first described by Robson, Shoemaker, Ogilvie & Manor (1973). Its crystal structure corresponds to a hypothetical structure proposed by Meier & Kokotailo (1965), which consists of a body-centered arrangement of α-cages in a cubic unit cell, linked by double eight-rings forming two separate but symmetrically dependent three-dimensional channel systems. Zeolite rho has achieved wide attention because of its highly flexible framework structure and because of its extraordinary role as a heterogeneous catalyst for the catalytic and shape-selective synthesis of methylamines from methanol and ammonia (Keane, Sonnichsen, Abrams, Corbin, Gier & Shannon, 1987; Gier, Shannon & Sonnichsen, 1986; Abrams, Gier, Shannon & Sonnichsen, 1986). It has been studied in the as-synthesized Na,Cs form as well as in various cation-exchanged modifications. It exhibits an extremely high flexibility with a cubic lattice constant a ranging from 13.9645 (7) Å in space group $I\bar{4}3m$ [Ca,D-rho (Corbin, Abrams, Jones, Eddy, Harrison, Stucky & Cox, 1990)] to 15.0976 (4) Å in space group $Im\bar{3}m$ [D-rho (Baur, Fischer, Shannon, Staley, Vega, Abrams, Corbin & Jorgensen, 1987)].

Even though it is used as a catalyst for the synthesis of methylamines, little is known about the crystal structures of the methylamine-loaded forms of zeolite rho. Meyer (1994) examined the sorption process of trimethylamine and water in a silicon-rich variety of zeolite Na,Cs-rho with a Si/Al ratio of $\sim$ 5:1. Our aim is to describe the sorption behavior of three variants of the methylamines, mono- (MMA), di- (DMA) and trimethylamine (TMA) in the catalytically active form of zeolite rho, *i.e.* in the ammonium-exchanged and subsequently deammoniated and dehydrated hydrogen forms of the zeolite. The first part of this series is concerned with monomethylamine adsorbed in zeolite rho.

2. Experimental

2.1. *Sample preparation*

All samples were prepared from Na,Cs-rho using AlOOH (Catapal SB), NaOH, CsOH and Ludox LS-30® according to the method described by Robson *et al.* (1973). The initial gel was aged for 5 d at 293 K and subsequently kept at 373 K for 6 d. Two batches of the zeolite were synthesized. One batch (series I) was treated six times with 10% NH_4NO_3 to exchange Na and Cs ions by ammonium. Experimental details are

† Part of this work was carried at the Institut für Geowissenschaften der Universität Mainz, Germany.

‡ Contribution No. 7364.

ISSN 0108-7681

Table 1. *Methylamine (MA) loadings in the zeolite rho samples*

Series I: Shallow bed calcined at 873 K under dry nitrogen, water content determined by TG analysis in the temperature range between room temperature and 673 K (sample Rho-I-9MMA between room temperature and 623 K), methylamine content between 673 and 973 K; series II: shallow bed calcined under steam at 773 K, water determined between room temperature and 573 K, methylamine content between 573 and 1073 K.

Sample series	Initial loading (no. per unit cell)	Weight loss of H_2O (mg)	No. of H_2O per unit cell*	Weight loss of MA (mg)	No. of MA per unit cell*	Desorption temperature (K)
Rho-I	5 MMA	12.2	27.8	4.2	5.9	723
Rho-I	9 MMA	5.9	24.5	3.5	8.2	713
Rho-II	5 MMA	3.3	23.2	0.7	2.7	643

* The number N of sorbed molecules is calculated according to $N = (M_Z WL_S/W_Z M_S)$, with the molar weight M_Z of the empty zeolite, the weight loss WL_S upon desorption, the weight W_Z of the zeolite after desorption and the molar weight M_S of the sorbate molecule.

given by Baur *et al.* (1987), who studied the hydrogen form of this zeolite. The NH_4-zeolite was calcined under shallow bed conditions in dry nitrogen at 873 K. X-ray fluorescence (XRF) analysis (Philips PW 1404) showed the aluminosilicate composition to be $Al_{11.2}Si_{36.8}O_{96}$, which agrees well with the mean composition stated in the former study. There, the Cs content was determined to be 0.2 atoms per unit cell. Quantitative ^{27}Al and ^{29}Si MAS NMR measurements (Baur *et al.*, 1987) indicated a considerable dealumination of the framework. The total number of Al atoms residing in tetrahedral framework sites is given as nine atoms per unit cell, as determined from the NMR experiments and NH_3 microcalorimetry. Consequently, the composition of the NH_4 precursor can be given as $(NH_4)_{11.0}Cs_{0.2}Al_{11.2}Si_{36.8}O_{96}$ and the composition of the calcined and dealuminated zeolite as $H_{8.8}Cs_{0.2}Al_9Si_{39}O_{96}.Al_2O_3$ in its anhydrous form.

The second batch (series II) was treated as described by Fischer, Baur, Shannon, Staley, Abrams, Vega & Jorgensen (1988), who studied the steam-calcined form of the zeolite. The Na,Cs-Rho was exchanged four times in 10% NH_4NO_3 solution to yield a unit-cell content of $(NH_4)_{10.5}Cs_{0.7}Al_{11.2}Si_{36.8}O_{96}$, as determined in the present work by XRF analysis. It agrees with the former determination within 0.1 atom per unit cell. The hydrogen form was prepared by heating NH_4-rho to 773 K for 1 h under rapidly flowing N_2 (1000 cm^3 min^{-1}) and then maintaining the sample at 773 K for 4 h under steam with 1000 cm^3 min^{-1} N_2 equilibrated to provide 81.5 kPa H_2O. From ^{29}Si and ^{27}Al MAS NMR spectroscopy (Fischer *et al.*, 1988), the number of framework Al atoms was determined to be six Al atoms per unit cell, yielding the composition $H_{5.3}Cs_{0.7}Al_6Si_{42}O_{96}.2.5Al_2O_3$ of the anhydrous zeolite.

Subsequently, three samples were prepared with different loadings of deuterated MMA. The hydrogen forms of the zeolites were placed into cells and heated up to 633 K under vacuum. They were maintained at 633 K for 16 h and then cooled to 573 K and exposed to 9 Torr of D_2O vapor in several cycles of exposure. After weighing, the sealed samples were placed back on the vacuum manifold, heated to 573 K and exposed to a defined amount of perdeutero-MMA to yield the initial loadings according to the data in Table 1. These samples are designated as dehydrated samples, used for neutron diffraction in their deuterated forms. After the neutron diffraction experiments, the samples were exposed to air and subsequently studied by X-ray diffraction in their hydrated forms. The methylamines are expected to be associated with the H (D) atoms of the hydrogen zeolite to form ionic groups of H-MMA^+ or D-MMA^+.

2.2. *Thermal analyses*

Differential thermal analyses (DTA) and thermogravimetric analyses (TG) were performed with Linseis L 81 thermal equipment. Measurements were carried in air with a heating rate of 10 K min^{-1}. Al_2O_3 was used as a reference material.

2.3. *X-ray diffraction*

X-ray diffraction data were collected at room temperature with an automatic powder diffractometer Seifert XRD ISO DEBYEFLEX 3000 with automatic divergence slit attachment (ADS). The ADS data show lower backgrounds, better peak-to-noise ratios and they do not suffer from beam overflow effects in the low 2θ region. However, for subsequent analyses, ADS intensities I_{ADS} have to be transformed into fixed slit intensities I_{FDS} using the conversion algorithm given by Fischer (1994)

$$I_{FDS} = I_{ADS}(\gamma_{FDS}\cos\theta/2\sin\theta)\{[(R^2/l^2\cos^2\theta) + 1]^{1/2} - (R/l\cos\theta)\}^{-1},$$

with the aperture γ_{FDS} (°) of the assumed FDS, the length l (mm) of the sample and the goniometer radius R (mm). Experimental conditions are summarized in Table 2.

Heating experiments were performed under *in situ* conditions with a Paar HTK 10 heating chamber attached to an automated Philips goniometer. Data were collected between 24.5 and 27.2° 2θ in steps of 0.03° with 5 s per step, which gives sufficient information for the analyses of suspected phase transitions. The sample was placed on a platinum heating plate with an attached thermocouple. The temperature gradient is *ca* 313–343 K between the surface of the platinum plate and the surface of the sample. The temperature gradient in the horizontal

Table 2. *Experimental conditions of data collection*

X-ray diffraction	
Radiation type, source	X-ray, Cu $K\alpha$
Instrumental settings	40 kV, 30 mA
Discriminator	Diffracted beam, curved graphite monochromator
Detector	Scintillation counter
Divergence slit	ADS
Receiving slit (mm)	0.2
Data collection temperature	Room temperature
Particle size (μm)	< 10
2θ range (°)	4–110
2θ step size (°)	0.03
Data collection mode	Step scan
Sample holder	Round sample holder (diameter 26 mm) with silicon single crystal bottom plate
Background correction	Spline interpolation between refined background grid points
Counting time per step (s)	10
Weighting scheme	$w = 1/y_{obs}$
Neutron diffraction	
Diffractometer	D2B (ILL Grenoble)
Wavelength (Å)	1.5946
Collimator	5′
Take-off angle (°)	135
Beam line (m)	14
Detector	64 He detectors
Data collection temperature (K)	5

direction from center to fringe is *ca* 308 K in the temperature range up to 1073 K.

2.4. *Neutron diffraction*

Neutron diffraction experiments were performed on the D2B instrument at the Institut Laue–Langevin (ILL) in Grenoble, France. All samples were filled into vanadium containers (diameter 11 mm, length 60 mm) and sealed with indium o-rings. The steel caps were shielded with cadmium. Experimental conditions are summarized in Table 2.*

2.5. *Computations*

Rietveld refinements [Rietveld (1969), modified versions by Wiles & Young (1981) and Hill & Howard (1986)], were performed with the Philips *PC-Rietveld plus* program package (Fischer, Lengauer, Tillmanns, Ensink, Reiss & Fantner, 1993) and an extensively modified version for incorporating distance least-squares (DLS) calculations (Meier & Villiger, 1969) into the refinement procedure (Kassner, 1993). In the DLS calculations the N—C distances were restrained to 1.463 Å using values from Thomas (1975), framework distances for Series I samples were restrained to T—O = 1.633 and O—O = 2.667 Å based on the Si/Al ratio using Si—O = 1.607 Å after Baur (1978) and Al—O = 1.746 Å after Baur & Ohta (1982). The distances for Series II samples are restrained to T—O = 1.624 and O—O = 2.653 Å, except for Rho-II-5MMA X and N(1) where framework atoms could be refined independently. X-ray scattering factors in their respective valence states were taken from the *International Tables for X-ray Crystallography* (1974, Vol. IV) and the values for O^{2-} from Hovestreydt (1983). The coherent neutron scattering lengths used in the refinements are b(Si) = 4.1491, b(Al) = 3.449, b(O) = 5.803, b(D) = 6.67, b(Cs) = 5.42, b(N) = 9.40 and b(C) = 6.648 fm (Koester, 1977). Background values were defined by spline interpolation between refinable set points. The crystal structure drawings were made with a modified version of the plotting program *STRUPLO* (Fischer, Le Lerzin, Kassner & Rüdinger, 1991). The contour map of the difference-Fourier calculations was drawn with a new program module (Auernhammer, unpublished program) in the *PC-Rietveld plus* package (Fischer, Lengauer, Tillmanns, Ensink, Reiss & Fantner, 1993).

The Caglioti equation (Caglioti, Paoletti & Ricci, 1958) with three variable parameters was used for the determination of full width at half-maximum (FWHM).

3. Results

3.1. *Thermal analyses*

The reactions and weight losses for the differently loaded samples are shown in Fig. 1 and the corresponding data are given in Table 1. All samples show an endothermal reaction in the thermal analyses around 373 K with a weight loss due to the desorption of water. Further weight loss with exothermal reactions between 573 and 773 K is due to the desorption of the methylamine. The molecules decompose leaving a residue of methyl groups, which is burned off above *ca* 823 K. The results of the thermal analyses differ slightly from the expected number of sorbed molecules in the initial preparation. This may be due to the fact that the reactions of water desorption, methylamine decomposition and desorption overlap and therefore make the exact determination of the number of sorbed molecules difficult. An underestimation of the methylamine content could be due to a sluggish desorption of MMA after keeping the samples for several months in the vanadium containers before they were thermally analysed.

3.2. *Rietveld analyses*

X-ray diffraction experiments were performed on the hydrated samples and neutron diffraction experiments on the dehydrated deuterium forms of the zeolites. Initial values for the atom coordinates in space group $Im\bar{3}m$ were taken from Fischer *et al.* (1988) and the starting values for space group $I\bar{4}3m$ from Fischer, Baur,

* The numbered intensity of each measured point has been deposited with the IUCr (Reference: SE0199). Copies may be obtained through The Managing Editor, International Union of Crystallography, 5 Abbey Square, Chester CH1 2HU, England.

Shannon, Parise, Faber & Prince (1989). The initial space groups were assigned based on the observation (Parise, Gier, Corbin & Cox, 1984; Parise, Abrams, Gier, Corbin, Jorgensen & Prince, 1984) that zeolites rho with lattice constants $a > 14.95$ Å crystallize in space group $Im\bar{3}m$ and those with smaller constants in $I\bar{4}3m$. In cases where the temperature factors did not converge to stable values, the B values of the O atoms were constrained to be equal, the temperature factors of nonframework atoms were fixed on $B = 5$ Å^2. In the hydrated samples it cannot be distinguished between water molecules and n.f.a. (nonframework alumina) species, which are statistically distributed on the same site. Refinements were performed using the oxygen scattering factor; consequently, some refined occupancies of water positions are much higher than expected from the thermal analyses. Since the nature of the n.f.a. species is not known exactly, the occupancies were not constrained to specific values. However, the high occupancies and the occurrence of the same sites in the dehydrated samples yield direct evidence for the n.f.a. species.

3.2.1. *Rho-I-5MMA X.* Refinements were performed in space group $Im\bar{3}m$. The lattice constant of $a = 14.9991\,(2)$ Å indicates that the crystal structure approaches noncentrosymmetric symmetry. However, refinements in $I\bar{4}3m$ yielded coordinates which are essentially identical within a few standard deviations to their centrosymmetric counterparts. Therefore, the results are given for the higher symmetry $Im\bar{3}m$.

In order to locate the sorbate molecules in the zeolite cavities the following steps were performed. Firstly, the

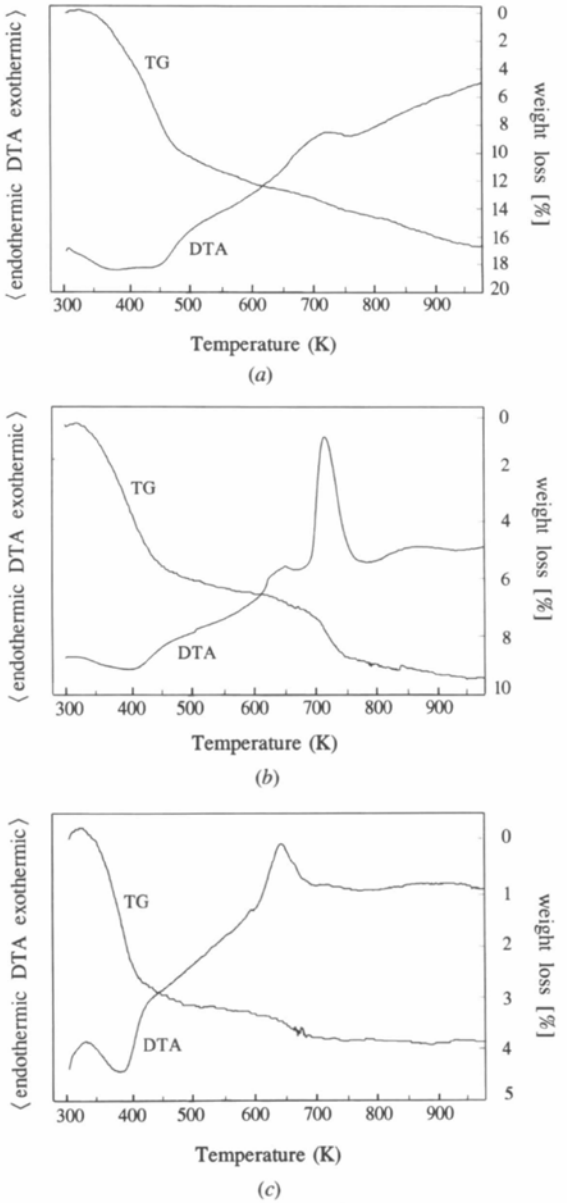

Fig. 1. Thermal reactions recorded by DTA and weight loss determined by TG: (*a*) Rho-I-5MMA; (*b*) Rho-I-9MMA; (*c*) Rho-II-5MMA.

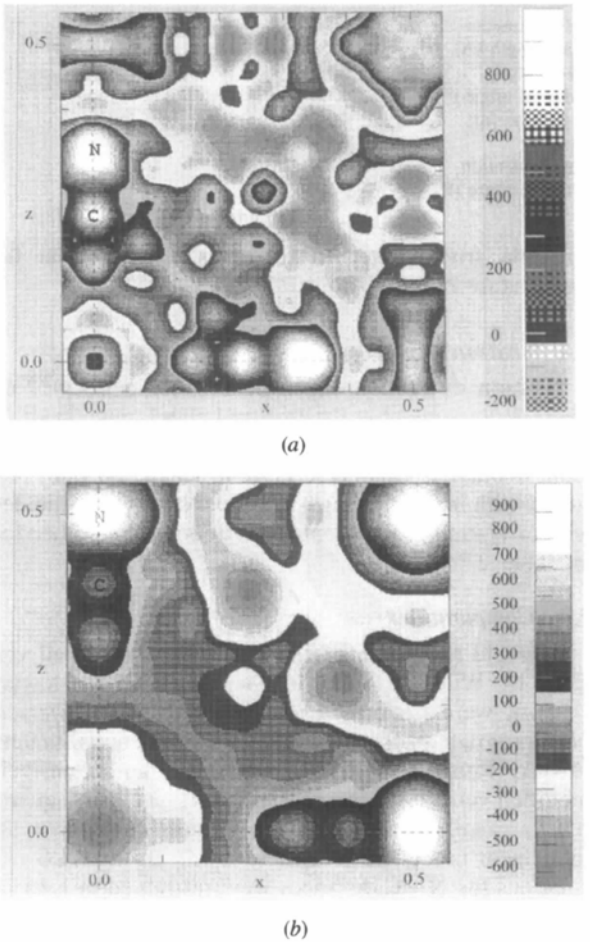

Fig. 2. Difference Fourier maps of Rho-I-5MMA in the layer $y = 0$ with F_{obs} values from X-ray and neutron diffraction data and F_{calc} values from the corresponding refinements of framework atoms. The highest maximum is scaled to 999. The positions of the molecules are indicated by the labels for the N and C atoms: (*a*) Rho-I-5MMA X; (*b*) Rho-I-5MMA N (1).

atom positions of the zeolite framework were refined using intensity data in the 2θ region between 50 and 110° only. These intensities are least affected by the molecules and therefore represent the main contribution of the framework structure. This is expressed by the resulting residuals of R_{wp} = 0.085 and R_B = 0.128, which essentially reflect the pure framework contribution in the high 2θ region. Subsequently, the structure factors were calculated using the full range in 2θ between 5 and 110°, with coordinates fixed at their previous values. This yielded residuals of R_{wp} = 0.916 and R_B = 0.982. The highest maxima in subsequently calculated difference-Fourier maps (Fig. 2*a*) are *ca* 1.5 Å apart. They were assigned to N (0, 0, 0.33) and C (0, 0, 0.23) atoms of the MMA molecule. In subsequent refinements the occupation factors of N and C were held at five atoms per unit cell. The residuals dropped to R_{wp} = 0.805 and R_B = 0.806 after incorporation of the MMA positions into the refinements. It should be noted that the high values of the initial residuals are due to the fact that the framework positions were held fixed at the positions determined from the refinements which were performed in the high 2θ region. Therefore, the values represent just the relative changes in the refinement steps and they do not reflect the actual goodness-of-fit. Residual electron densities were assigned to water positions and to the Cs atom. Their incorporation into the refinement yielded residuals of R_{wp} = 0.351 and R_B = 0.377, which further dropped to R_{wp} = 0.095 and R_B = 0.073 after refining the profile and atomic parameters. The intramolecular distances in the methylamines were restrained by geometrical soft constraints in the combined Rietveld and DLS refinement. This is an appropriate approach since the geometry of the molecules is known and it is not expected that the configuration will change in the zeolite channels. However, the procedure allows the determination of the molecule position as well as free rotations of the rigid molecule. That way, the number of parameters in the least-squares procedure can be reduced without any loss of information, provided that the symmetry and configuration of the molecules are known. Subsequent difference-Fourier analyses yielded positions which were assigned to water molecules.

3.2.2. *Rho-I-5MMA N.* The analysis of the dehydrated sample Rho-I-5MMA by neutron diffraction studies proceeded similarly. However, shoulders on all reflection peaks in the powder pattern indicate that the sample consists of two zeolite rho phases. Both phases crystallize in $I\bar{4}3m$ with lattice constants a = 14.8410 (7) and 14.5273 (11) Å, clearly below the transition point between 14.9 and 15.0 Å, where the centrosymmetric structure transforms to the noncentrosymmetric form. The coexistence of two phases definitely complicates the analysis. However, difference Fourier maps (Fig. 2*b*) directly revealed the MMA positions in both phases with the higher maximum close to the center of the double eight-ring assigned to N. A statistical distribution of N and Cs atoms on the same site was assumed which yielded a refined value of 5.15 (5) N atoms per unit cell in phase (1) and 5.0 (1) N atoms in phase (2), which is in good agreement with the number of sorbed molecules (5.9 as determined by TG experiments, Table 1). The molar fractions of the two phases calculated from the refined scale factors are 60% for phase 1 and 40% for phase 2. The second maximum in the difference Fourier map has a distance of *ca* 1.5 Å to the N atom and therefore has been assigned to the C atoms of the MMA molecule. The refinement improved further with the incorporation of three-dimensional atoms in the methyl group, which were constrained to prescribed distances in the refinements. Another peak appears in the Fourier map which cannot be assigned to any of the nonframework atoms. Although the quality of this two phase data set does not provide data with the accuracy of single-phase analyses, the refinements show an improvement in the R_B values of 6% in both phases upon incorporation of this position which clearly indicates significant scattering matter on this site. Its crystal chemical environment with distances of *ca* 3.2 Å to framework O atoms could be interpreted assuming water molecules which also occur as *W*1 sites in the hydrated samples. Although the existence of water is unlikely from the preparation conditions, water could have diffused through small leaks of the sample can. Another possible interpretation is the assignment to n.f.a. condensed to form a neutral Al_2O_3 or AlOOH complex, as discussed by Shannon, Staley, Vega, Fischer, Baur & Auroux (1989) for zeolite rho. Strong evidence for such n.f.a. species is given by the ^{29}Si and ^{27}Al MAS NMR results of the former studies (Baur *et al.*, 1987) of the same sample in its unloaded hydrogen (deuterium) form. The total number of tetrahedrally and octahedrally coordinated Al cannot be inferred unambiguously from the NMR experiments due to site-symmetry distortions yielding very broad NMR signals. However, the results clearly indicate that n.f.a. species have formed during calcination, located in the big cavities of the zeolite weakly attached to framework sites. Such Al_2O_3 complexes will be highly disordered in the zeolite cages and do not allow a detailed analysis of the atomic positions. The fact that similar positions were observed in all further studies of this series as well (Rho-II-5MMA N, this work; Rho-I-5TMA N and Rho-II-5TMA N, part III) makes it unlikely that all sample cans should have leaked or that water has been introduced despite careful sample handling. Therefore, the scattering density observed in the anhydrous form of the zeolites is considered to be related to the nonframework aluminum species. This implies that water molecules determined in the X-ray diffraction experiments of the hydrated zeolites might also be involved in the n.f.a. formation (see also *Discussion* in part III of this series). In Table 4

Table 3. *Crystal data [space group, lattice constant a, volume V, framework density FD (no. of T atoms per 1000 Å^3), channel aperture A, ellipticity parameter Δ_e] and residuals*

X-ray diffraction data and neutron diffraction data Rho-I-5MMA N and Rho-II-5MMA N consist of two zeolite rho phases (first and second line for the respective entries).

	Rho-I			Rho-II	
	5 MMA X-ray	5 MMA Neutron	9 MMA X-ray	5 MMA X-ray	5 MMA Neutron
Space group	$Im\bar{3}m$	$I\bar{4}3m$ $I\bar{4}3m$	$I\bar{4}3m$	$Im\bar{3}m$	$I\bar{4}3m$ $I\bar{4}3m$
a (Å)	14.9991 (2)	14.8410 (7) 14.5273 (11)	14.9771 (2)	15.0323 (2)	14.9151 (2) 14.6475 (8)
V (Å^3)	3374.4	3268.8 3065.9	3359.6	3396.8	3318.0 3142.6
FD (10^{-3}Å^{-3})	14.22	14.68 15.66	14.29	14.13	14.47 15.27
A (Å)*	3.64	3.16 2.63	3.75	3.88	3.34 2.86
Δ_e†	1	1.44 1.73	1.20	1	1.37 1.58
R_{wp}‡	0.095	0.038	0.090	0.124	0.031
R_B‡	0.073	0.083 0.074	0.057	0.049	0.061 0.076

* Apertures represent the smallest diameters of the channels as defined by Baur & Fischer (1997). For the structures in $I\bar{4}3m$ this is the distance between two O3 atoms across the channel in the direction [110] reduced by the ionic radius of an O atom (2 × 1.35 Å), calculated by $A = [8^{1/2}x(\mathrm{O3})]a - 2.7$. The aperture for the centrosymmetric structures in $Im\bar{3}m$ is calculated in the direction [100] by measuring the distance between two O1 atoms across the channel yielding $A = 2y(\mathrm{O1})a - 2.7$. † Ellipticity parameter after Baur, Fischer & Shannon (1988). $\Delta_e = x(\mathrm{O2})/x(\mathrm{O3})$. ‡ Residuals: $R_{wp} = [\Sigma_i w_i(y_{io} - Cy_{ic})^2/\Sigma w_i y_{io}^2]^{1/2}$, $R_B = \Sigma_k|I_{ko} - CI_{kc}|/\Sigma_k I_{ko}$, where R_{wp} = weighted residual including profile intensities; R_B = residual including integrated intensities; y_o, y_c = observed and calculated profile intensities; I_o, I_c = observed and calculated integrated intensities; C = scale factor; w = weight = $1/y_o$.

Table 4. *Atom positions in fractional coordinates*

Isotropic displacement factors (Å^2) and occupancies given in number of atoms per unit cell.

Sample position	Atom	x	y	z	B (Å^2)	Atoms per unit cell	Wyckoff position
(*a*) Compounds with space group $Im\bar{3}m$							
Rho-I-5 MMA X	Si/Al	1/4	0.1032 (1)	$1/2 - y$	2.02 (5)	39/9	(48*i*)
Rho-II-5 MMA X	Si/Al	1/4	0.1025 (2)	$1/2 - y$	2.12 (6)	42/6	(48*i*)
Rho-I-5 MMA X	O1	0	0.2115 (3)	0.3850 (2)	4.3 (1)	48	(48*j*)
Rho-II-5 MMA X	O1	0	0.2190 (4)	0.3811 (3)	1.6 (1)	48	(48*j*)
Rho-I-5 MMA X	O2	0.1710 (2)	x	0.3764 (3)	B(O1)	48	(48*k*)
Rho-II-5 MMA X	O2	0.1615 (2)	x	0.3724 (4)	4.8 (2)	48	(48*k*)
Rho-I-5 MMA X	Cs	0	0	0.456 (1)	5	0.8 (1)*	(12*e*)
Rho-II-5 MMA X	Cs	0	0	0.434 (1)	5	0.9 (1)	(12*e*)
Rho-I-5 MMA X	*W*1	0	0	0.338 (1)	5	6.2 (1)*	(12*e*)
Rho-II-5 MMA X	*W*1	0	0	0.323 (2)	5	5.5 (2)	(12*e*)
Rho-I-5 MMA X	*W*2/*X*†	0.0345 (9)	0.0933 (7)	0.2417 (6)	5	22.6 (2)	(96*l*)
Rho-I-5 MMA X	*W*3	0.1499 (6)	x	0.117 (1)	5	14.5 (1)	(48*k*)
Rho-II-5 MMA X	*W*3	0.166 (1)	x	x	5	6.8 (2)	(16*f*)
Rho-I-5 MMA X	*W*4	0.0714 (5)	x	x	5	7.3 (1)	(16*f*)
Rho-II-5 MMA X	*W*4	0.041 (2)	0.075 (1)	0.1801 (8)	5	14.9 (2)	(96*l*)
Rho-I-5 MMA X	N	0	0	0.3623 (7)	5	5	(12*e*)
Rho-II-5 MMA X	N	0	0	0.3475 (7)	5	5	(12*e*)
Rho-I-5 MMA X	C	0	0	0.2651 (7)	5	5	(12*e*)
Rho-II-5 MMA X	C	0	0	0.2503 (7)	5	5	(12*e*)
(*b*) Compounds with space group $I\bar{4}3m$							
Rho-I-5 MMA N(1)	Si/Al	0.2640 (3)	0.1139 (3)	0.4129 (3)	2.35 (3)	39/9	(48*h*)
Rho-I-5 MMA N(2)	Si/Al	0.2734 (4)	0.1233 (4)	0.4269 (4)	5.5 (3)	39/9	(48*h*)
Rho-I-9 MMA X	Si/Al	0.2574 (3)	0.1095 (2)	0.4051 (2)	1.34 (4)	39/9	(48*h*)
Rho-II-5 MMA N(1)	Si/Al	0.2630 (2)	0.1151 (3)	0.4124 (2)	1.32 (6)	42/6	(48*h*)
Rho-II-5 MMA N(2)	Si/Al	0.2698 (4)	0.1179 (4)	0.4218 (4)	5.4 (3)	42/6	(48*h*)
Rho-I-5 MMA N(1)	O1	0.0208 (3)	0.2149 (4)	0.3884 (4)	3.5 (1)	48	(48*h*)
Rho-I-5 MMA N(2)	O1	0.0379 (4)	0.2082 (5)	0.3900 (5)	2.76 (7)	48	(48*h*)
Rho-I-9 MMA X	O1	0.0100 (3)	0.2160 (3)	0.3825 (2)	3.0 (1)	48	(48*h*)

Table 4 (*cont.*)

Rho-II-5 MMA N(1)	O1	0.0179 (2)	0.2107 (2)	0.3863 (2)	1.40 (2)	48	(48*h*)
Rho-II-5 MMA N(2)	O1	0.0300 (4)	0.2070 (5)	0.3905 (5)	3.5 (1)	48	(48*h*)
Rho-I-5 MMA N(1)	O2	0.2003 (4)	*x*	0.3857 (7)	3.9 (1)	24	(24*g*)
Rho-I-5 MMA N(2)	O2	0.2245 (4)	*x*	0.4066 (6)	B(O1)	24	(24*g*)
Rho-I-9 MMA X	O2	0.1828 (3)	*x*	0.3715 (5)	B(O1)	24	(24*g*)
Rho-II-5 MMA N(1)	O2	0.1955 (2)	*x*	0.3823 (4)	1.77 (6)	24	(24*g*)
Rho-II-5 MMA N(2)	O2	0.2121 (5)	*x*	0.4002 (7)	2.8 (2)	24	(24*g*)
Rho-I-5 MMA N(1)	O3	0.1396 (4)	*x*	0.6188 (6)	3.5 (2)	24	(24*g*)
Rho-I-5 MMA N(2)	O3	0.1297 (5)	*x*	0.6166 (5)	B(O1)	24	(24*g*)
Rho-I-9 MMA X	O3	0.1523 (3)	*x*	0.6277 (5)	B(O1)	24	(24*g*)
Rho-II-5 MMA N(1)	O3	0.1431 (2)	*x*	0.6221 (2)	1.75 (6)	24	(24*g*)
Rho-II-5 MMA N(2)	O3	0.1341 (5)	*x*	0.6173 (7)	2.5 (2)	24	(24*g*)
Rho-I-5 MMA N(1)	Cs	0	0	1/2	5	0.2	(6*b*)
Rho-I-5 MMA N(2)	Cs	0	0	1/2	5	0.2	(6*b*)
Rho-I-9 MMA X	Cs	0	0	1/2	5	0.55 (5)	(6*b*)
Rho-II-5 MMA N(1)	Cs	0	0	1/2	5	0.7	(6*b*)
Rho-II-5 MMA N(2)	Cs	0	0	1/2	5	0.7	(6*b*)
Rho-I-5 MMA N(1)	*W*2/*X*‡	0.011 (2)	0.048 (1)	0.251 (1)	5	12.0	(48*h*)
Rho-I-9 MMA X	*W*2/*X*‡	0.0582 (4)	*x*	0.2334 (6)	5	18.7 (1)	(24*g*)
Rho-II-5 MMA N(1)	*W*2/*X*‡	0.010 (1)	0.0510 (9)	0.2518 (7)	5	10.7 (1)	(48*h*)
Rho-I-9 MMA X	*W*3	0.1583 (6)	*x*	0.1063 (9)	5	14.4 (1)	(24*g*)
Rho-I-9 MMA X	*W*4	0.098 (1)	*x*	0.041 (2)	5	4.8 (1)	(24*g*)
Rho-I-5 MMA N(1)	N	0	0	1/2	5	5.15 (5)	(6*b*)
Rho-I-5 MMA N(2)	N	0	0	0.4871 (7)	5	5.0 (1)	(12*e*)
Rho-I-9 MMA X	N	0	0	0.3918 (6)	5	9	(12*e*)
Rho-II-5 MMA N(1)	N	0	0	0.4864 (6)	5	5	(12*e*)
Rho-II-5 MMA N(2)	N	0	0	1/2	5	5	(6*b*)
Rho-I-5 MMA N(1)	C	0	0	0.4027 (4)	5	Occ (N)	(12*e*)
Rho-I-5 MMA N(2)	C	0	0	0.3864 (7)	5	Occ (N)	(12*e*)
Rho-I-9 MMA X	C	0	0	0.2951 (6)	5	9	(12*e*)
Rho-II-5 MMA N(1)	C	0	0	0.3884 (6)	5	5	(12*e*)
Rho-II-5 MMA N(2)	C	0	0	0.4001 (6)	5	5	(12*e*)
Rho-I-5 MMA N(1)	D1	0.0011 (9)	0.0613 (6)	0.3810 (4)	5	Occ (N)	(48*h*)
Rho-I-5 MMA N(1)	D2	0.0523 (6)	0.0317 (8)	0.3810 (4)	5	Occ (N)	(48*h*)
Rho-I-5 MMA N(1)	D3	0.0536 (6)	0.0288 (8)	0.3810 (4)	5	Occ (N)	(48*h*)

* Occupancies constrained to give a total of 12 atoms in the sum of Cs, *W*1 and MMA with a fixed number of five MMA molecules. † In the dehydrated samples, the *X* position is assigned to n.f.a. species. Statistical distribution of water molecules and n.f.a. species (*x*) on the same site is assumed. Refinement is based on the O scattering factor only. ‡ These positions correspond to water and n.f.a. sites in the hydrated samples. In the dehydrated samples we essentially assume occupation by n.f.a. species. Occ refers to occupancy dependent on atom given in parentheses.

the position X, given together with the *W*2 position is assigned to n.f.a. species.

3.2.3. *Rho-I-9MMA X.* The refinement was performed analogously to Rho-I-5MMA. The highest maximum in the difference-Fourier map appeared at 0, 0, $\frac{1}{2}$, but the refinement of an N atom on this position yielded negative occupancies. Placing N on the 0, 0, *z* position towards the single eight-ring gave positive values on a site close to the center of the single eight-ring. The central position in the double eight-ring was assigned to Cs. The methyl groups (C atoms in the refinement) point towards the center of the α-cage. After incorporation of the water positions, the refinements converged at the residuals given in Table 3.

3.2.4. *Rho-II-5MMA X.* Initial analyses of the powder diffraction data showed that the zeolite rho phase coexists with a chabazite impurity with a content of *ca* 5 mol %, as determined from the Rietveld scale factors. Subsequently, the chabazite lines were simulated based on the crystal structure data given by Smith, Rinaldi & Dent Glasser (1963). Only lattice constants, scale factors and profile parameters were refined simultaneously with the zeolite rho parameters. Difference-Fourier maps yielded a highest maximum in 0, 0, *z* with the N atom close to the center of the single eight-ring and the C atom pointing to the center of the α-cage. This orientation of the MMA molecule was adopted from the neutron diffraction analysis where the N and C atoms can be better distinguished by their different scattering length (C = 6.648, N = 9.40 fm) compared with the X-ray case, where N and C have similar scattering factors. The Cs atom resides on a position in the center of the single eight-ring. The close distance between N and Cs is avoided by the partial occupation of both sites.

3.2.5. *Rho-II-5MMA N.* As observed before for the sample Rho-I-5MMA N, the zeolite disproportionates into two zeolite rho phases upon dehydration and cooling. The molar fractions of the two phases calculated from the refined scale factors are 66% for phase (1) and 34% for phase (2). Chabazite impurities were treated as background. Difference-Fourier analyses revealed the MMA molecules in the center of the double eight-ring.

The results of the refinements are given in Tables 3 and 4, selected interatomic distances are listed in

Table 5. *Selected interatomic distances (Å) and angles (°)*

	Rho-I				Rho-II		
	5MMA X-ray	5MMA Neutron (1)	5MMA Neutron (2)	9MMA X-ray	5MMA X-ray	5MMA Neutron (1)	5MMA Neutron (2)
T—O1	1.662 (4) 2×	1.604 (7)	1.647 (9)	1.625 (5)	1.628 (6) 2×	1.623 (4)	1.626 (9)
T—O2	1.591 (4) 2×	1.643 (7)	1.659 (9)	1.646 (6)	1.643 (4) 2×	1.629 (5)	1.649 (9)
T—O3		1.632 (8)	1.633 (9)	1.625 (7)		1.630 (4)	1.628 (9)
T—O1		1.632 (7)	1.650 (8)	1.650 (5)		1.691 (5)	1.647 (9)
mean	1.627 (4)	1.628 (7)	1.647 (9)	1.637 (6)	1.636 (5)	1.643 (5)	1.638 (9)
O1—T—O1	108.6 (2)	107.0 (4)	108.8 (4)	111.0 (3)	111.7 (3)	108.8 (3)	109.2 (5)
O1—T—O2	111.7 (2) 2×	110.8 (4)	110.3 (5)	114.3 (3)	111.5 (2) 2×	106.4 (2)	108.3 (5)
O1—T—O2	108.4 (2) 2×	111.6 (5)	111.3 (5)	106.6 (3)	104.1 (2) 2×	115.2 (3)	110.9 (5)
O2—T—O2	108.1 (2)				114.1 (3)		
O1—T—O3		109.1 (5)	110.2 (5)	107.2 (4)		106.6 (2)	108.1 (5)
O1—T—O3		107.5 (4)	106.6 (5)	110.9 (3)		109.5 (3)	109.8 (5)
O2—T—O3		110.7 (5)	109.5 (5)	106.9 (3)		110.2 (3)	110.6 (6)
mean	109.5 (2)	109.5 (5)	109.5 (5)	109.5 (3)	109.5 (2)	109.5 (3)	109.5 (5)
N—O1	3.190 (3) 4×	3.607 (6) 8×	3.382 (8) 4×	3.242 (4) 4×	3.331 (4) 4×	3.490 (5) 4×	3.459 (6) 8×
N—O1			3.555 (8) 4×			3.681 (5) 4×	
N—O2	3.632 (3) 4×				3.453 (4) 4×		
N—O3		3.418 (7) 4×	3.06 (1) 2×	3.240 (5) 2×		3.425 (5) 2×	3.267 (9) 4×
N—O3			3.26 (1) 2×			3.634 (6) 2×	
C—O1	3.647 (8) 4×	3.211 (6) 4×	3.074 (6) 4×			3.154 (2) 4×	3.068 (6) 4×
C—O3		2.946 (7) 2×	2.665 (9) 2×	3.427 (6)		3.023 (3) 2×	2.790 (9) 2×

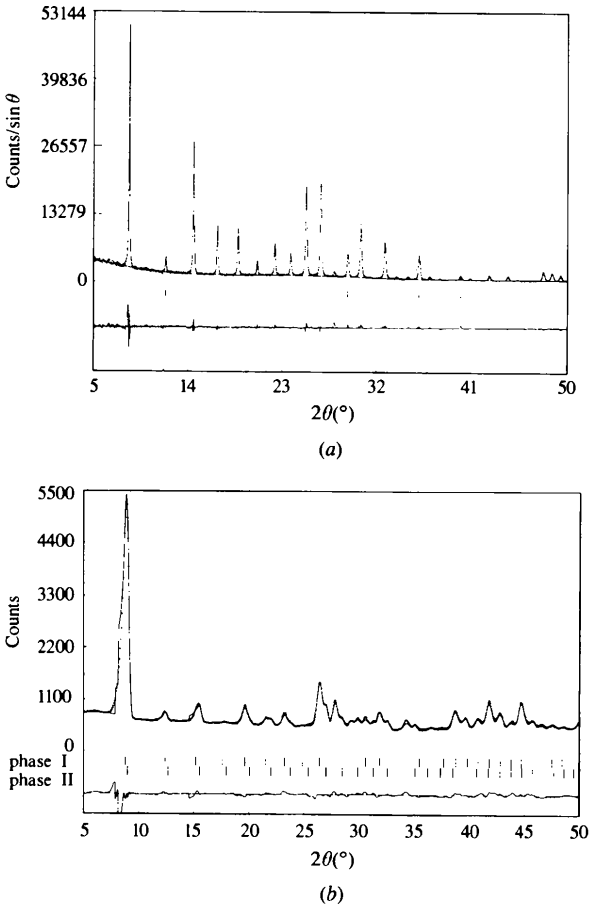

Fig. 3. Observed (+) and calculated (solid line) intensities with difference plot underneath. Theoretical peak positions are indicated by tick marks: (*a*) Rho-I-5MMA X; (*b*) Rho-I-5MMA N.

Table 5. The fit between observed and calculated powder diffraction data is shown in Fig. 3.

4. Discussion

4.1. *The (Si,Al)O_2-framework*

Zeolite rho exhibits an extremely flexible framework structure shown by the large variation of its lattice constant *a*, which directly expresses the variations in the T—O distances and O—T—O angles. In some cases the interatomic distances between framework atoms were restrained to prescribed values with different weights in the Rietveld refinements. However, this only affects the intrapolyhedral geometry of the TO_4 groups and not the joints between the tetrahedra. It permits the determination of the free diameters of the zeolite channels which determine the shape-selective properties of the zeolites. The minimum apertures for the zeolites studied here are given in Table 3, they are plotted *versus a* in Fig. 4. The values corresponding to the smaller lattice constants are in agreement with data known for zeolite rho (Baur & Fischer, 1997). A linear increase of the channel apertures is expected for the noncentrosymmetric structures, whereas the distribution of the values in space group $Im\bar{3}m$ is scattered over a wider range with a steeper slope. Data points beyond *ca* 14.9 Å deviate from the straight line of average values in $I\bar{4}3m$ and thus might represent an intermediate state between the centrosymmetric and noncentrosymmetric zeolites. However, the refinements indicate a preference for the noncentrosymmetric space group. A similar situation occurs for the ellipticity parameters Δ_c, which represent the elliptical distortion of the eight-rings. Fig. 5 shows

the Δ_e values plotted *versus* the lattice constant a with an approximately linear decrease until the data point for Rho-I-9MMA is encountered, which is shifted closer to the baseline representing the circular shape of the eight-ring.

4.2. *The water molecules*

Water molecules were assigned to positions derived from the difference-Fourier maps with distances to framework atoms within the range of hydrogen bonds. Incorporation of these positions into the refinements significantly improved the fit between observed and calculated data, as expressed by the decrease in the residuals. The water sites are only partially occupied and the molecules are statistically distributed over the equivalent positions. It should be considered that the coordinates given in Table 4 represent average positions only and therefore the standard deviations might not reflect the real deviations. However, crystal chemical information can be inferred from these data. *W*1 resides in the α-cage on the central axis of the eight-ring channel close to a single eight-ring. It has only weak bonds to O1 with distances 3.248 (6) Å in Rho-I-5MMA X. It disappears for the higher loadings with methylamines. *W*2 molecules were found in Rho-I and in Rho-II with 5 and 9 MMA around the central axis further down to the cage center. Due to the proximity to the 0, 0, z position [site (12*e*) in $Im\bar{3}m$ and $I\bar{4}3m$], *W*2 has two short distances, which limits the site occupation to 24 molecules per unit cell. The maximum loading is 22.6 (2) molecules in Rho-I-5MMA, which is close to the maximum amount of molecules permitted on this site. The water molecule has two distances within hydrogen-bonding values to framework O atoms (O1 and O2) and to other water molecules. *W*3 and *W*4 lie on positions in the inner part of the α-cage close to the threefold axis, which limits the loading to 16 molecules per unit cell. Refinement of the occupation yielded values close to the maximum occupation. *W*3 has a distance of 3.28 (1) Å to O3 in Rho-I-9MMA X and further contacts with *W*2 and *W*4 molecules. The water molecule *W*4 is bonded to only water molecules. It should be noted that some water positions might represent contributions from n.f.a. species, as mentioned above for the results of the dehydrated samples studied by neutron diffraction. Consequently, the number of refined water molecules exceeds the corresponding number determined by thermal analyses, as explained in the *Experimental*.

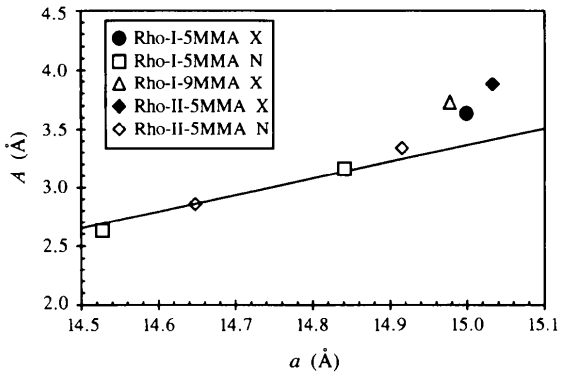

Fig. 4. Minimum apertures of the eight-ring channels defined by the eight-ring diameter in the direction [100] for the centrosymmetric structures and [110] for the noncentrosymmetric structures (for definitions see Table 3). Based on ionic oxygen (r = 1.35 Å). The straight line represents average values derived from the linear interpolation of all published centrosymmetric rho zeolites after Baur & Fischer (1997).

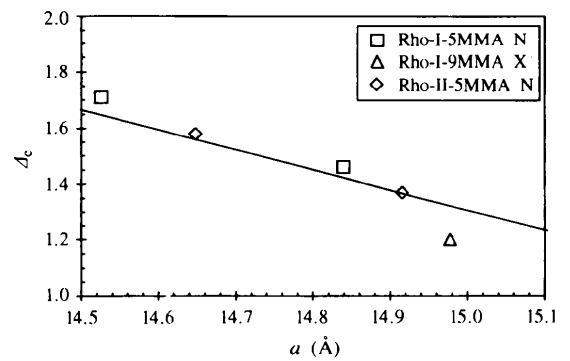

Fig. 5. Plot of ellipticity parameters Δ_e of eight-ring channels *versus* lattice constant a. The straight line represents average values derived from linear interpolation of all published centrosymmetric rho zeolites after Baur & Fischer (1997).

4.3. *The MMA molecule*

The intramolecular distances were prescribed by values given by Thomas (1975) defining the N—C restraints in the refinements. The N atom has a tetrahedral coordination with one methyl group and three protons (deuterons) with distances of 1.46 Å between the N and C atoms. The N atom resides in the α-cage on the central axis [0, 0, z] through the double eight-ring channels, as shown in Fig. 6. In the hydrated samples the molecule points with the N atom towards the center of the single eight-ring and with the C atoms towards the center of the α-cage. The distances between the N atoms and framework O atoms (Table 5) indicate hydrogen bonding or ionic interactions of the MMA^+ molecules with framework sites. The methyl groups point away from the framework atoms, which conforms with the repulsive behavior of CH_3 in an anionic framework. In the dehydrated samples the situation is different. The MMA penetrates the double eight-ring and achieves a closer contact with the methyl group to the framework with distances between 2.67 [Rho-I-5MMA N (2)] and 3.02 Å [Rho-II-5MMA N (1)] to framework O atoms.

4.4. *The effect of dehydration, cooling and heating*

Upon dehydration and cooling to 5 K the samples Rho-I-5MMA and Rho-II-5MMA disproportionate into two phases of zeolite rho, which undergo a phase transi-

tion from the centrosymmetric structure in $Im\bar{3}m$ [Rho-I-5MMA, a = 14.9991 (2) Å] to noncentrosymmetric phases in $I\bar{4}3m$ [Rho-I-5MMA, a = 14.8410 (7) and 14.5273 (11) Å]. Such a disproportionation has been observed before for zeolite Ca,ND_4-rho (Corbin *et al.*, 1990) and NH_4-rho (Bieniok & Baur, 1993).

In order to obtain more information on the temperature behavior of the sample, X-ray heating experiments of Rho-I-5MMA were performed with the Paar heating chamber. Data were collected at room temperature and subsequently in steps of 25 K up to 548 K. The temperature was held at 548 K overnight to ensure complete dehydration and then it was raised to 573 K. The sample was cooled down to room temperature again and heated in a second cycle in steps of 50 K (last step 100 K) to 873 K. Characteristic steps are shown in the powder patterns of Fig. 7. The 2θ positions of reflections 033/114 and 024 shift to higher values upon heating from room temperature to 523 K with gradually increasing peak widths. At 573 K a shoulder appears at the high 2θ side of the peaks, indicating the decomposition into two phases. Cooling down to room temperature leads to a rehydration of the sample with an X-ray pattern without split peaks. Reheating to 573 K again yields the split peaks and further heating to 873 K causes a shift of the reflections to lower values and a uniform peak shape of a single phase pattern above 723 K. Upon rehydration, the MMA molecules migrate from the center of the double eight-rings towards the α-cage. Similar results were obtained by Corbin *et al.* (1990) for Ca,ND_4-rho. Since the sample turns into a single phase in its dehydrated state above 723 K, the effects cannot be explained by simple hydration and dehydration mechanisms only. It is more likely that a redistribution of the MMA molecules occurs as a function of temperature and hydration. Describing the process from the initial room-temperature state, the zeolite decomposes to two phases with different lattice constants upon dehydration and turns into a single phase at elevated temperatures. These results show that the disproportionation is not an effect of cooling the zeolite down to 5 K, which could be suspected from the neutron diffraction experiments.

4.5. *The effect of different MMA loadings*

The sample Rho-I was studied with two different loadings of MMA sorbed with 5 and 9 molecules per unit cell, respectively. The decrease in the cell constants of 0.022 Å accompanied by a phase transition going from the centrosymmetric space group $Im\bar{3}m$ to the noncentrosymmetric space group $I\bar{4}3m$ upon increasing the loading from 5 to 9 molecules demonstrates the influence of the bonds between the MMA molecules and the framework atoms. Increasing the amount of molecules leads to a distortion of the framework with an elliptical deformation of the eight-rings expressed by the distortion index Δ_e = 1.2 (Table 3). The minimum aperture, though, shows the opposite effect. The aperture A distends from 3.64 to 3.75 Å when the amount of MMA is increased, that is increasing the number of MMA molecules expands locally the available space, but overall the unit cell is contracted due to the elliptical distortion of the eight-ring channels.

4.6. *The effect of differently prepared zeolite hosts*

The sample Rho-I was prepared by shallow-bed calcination of the NH_4-zeolite under dry nitrogen at 873 K,

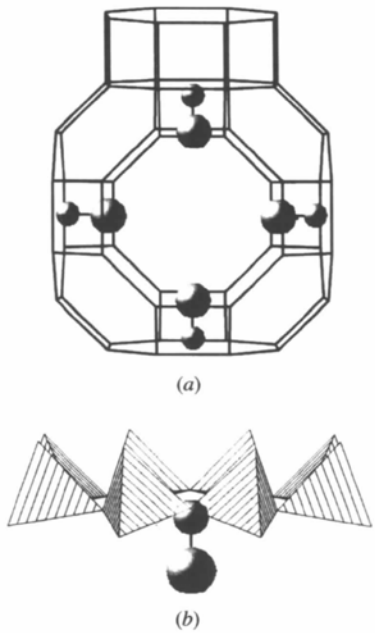

Fig. 6. Projection of the framework structure of Rho-I-5MMA as a skeleton model with the MMA molecule close to the single eight-ring. The large circles represent the C atoms (methyl groups), the smaller circles the N atoms.

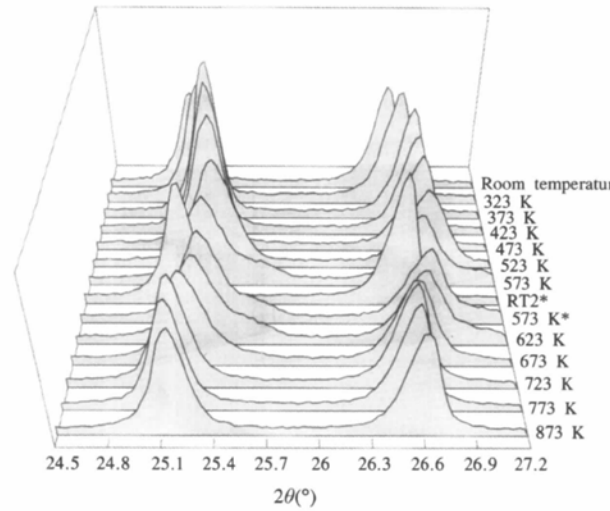

RT2*: cooled down to room temperature
573 K*: reheated to 573 K

Fig. 7. Diffraction patterns of Rho-I-5MMA recorded by *in situ* heating experiments at temperatures between room temperature and 873 K.

whereas Rho-II was steam-treated at 773 K to produce the hydrogen form. In all cases, the lattice constants of Rho-II are larger than the corresponding values of Rho-I. The changes in the lattice constants upon dehydration are slightly more pronounced in the series I samples than in the Rho-II series. In general, however, the behavior of the two samples is quite similar.

This work was supported by the Deutsche Forschungsgemeinschaft under grant Fi442/2. The Heisenberg fellowship to RXF is gratefully acknowledged. Computing time was provided by the Zentrum für Datenverarbeitung, University of Mainz. We thank U. Ciesla and W. Schmidt (University of Frankfurt) for the thermal analyses, N. Groschopf (University of Mainz) for support with the chemical analyses and W. H. Baur (University of Frankfurt) for his careful reading and numerous comments on the manuscript.

References

Abrams, L., Gier, T. E., Shannon, R. D. & Sonnichsen, G. C. (1986). European Patent Application 183 423.

Baur, W. H. (1978). *Acta Cryst.* B**34**, 1751–1756.

Baur, W. H. & Fischer, R. X. (1997). *Numerical Data and Functional Relationships in Science and Technology*. Landolt–Börnstein Series III, edited by W. H. Baur & R. X. Fischer, in preparation.

Baur, W. H. & Ohta, T. (1982). *Acta Cryst.* B**38**, 390–401.

Baur, W. H., Fischer, R. X., Shannon, R. D. (1988). *Innovation in Zeolite Materials Science. Studies in Surface Science and Catalysis*, edited by P. J. Grobet, W. J. Mortier, E. F. Vansant & G. Schulz-Ekloff, pp. 281–292. Amsterdam, Oxford, New York, Tokyo: Elsevier.

Baur, W. H., Fischer, R. X., Shannon, R. D., Staley, R. H., Vega, A. J., Abrams, L., Corbin, D. R. & Jorgensen, J. D. (1987). *Z. Kristallogr.* **179**, 281–304.

Bieniok, A. & Baur, W. H. (1993). *Acta Cryst.* B**49**, 817–822.

Caglioti, G., Paoletti, A. & Ricci, F. P. (1958). *Nucl. Instrum.* **3**, 223–228.

Corbin, D. R., Abrams, L., Jones, G. A., Eddy, M. M., Harrison, W. T. A., Stucky, G. D. & Cox, D. E. (1990). *J. Am. Chem. Soc.* **112**, 4821–4830.

Fischer, R. X. (1994). *Ber. Dtsch. Min. Ges. Beih. Eu. J. Mineral.* **6**, 63.

Fischer, R. X., Baur, W. H., Shannon, R. D., Parise, J. B., Faber, J. & Prince, E. (1989). *Acta Cryst.* C**45**, 983–989.

Fischer, R. X., Baur, W. H., Shannon, R. D., Staley, R. H., Abrams, L., Vega, A. J. & Jorgensen, J. D. (1988). *Acta Cryst.* B**44**, 321–334.

Fischer, R. X., Le Lirzin, A., Kassner, D. & Rüdinger, B. (1991). *Z. Kristallogr.* Suppl. Issue No. 3, 75.

Fischer, R. X., Lengauer, C., Tillmanns, E., Ensink, R. J., Reiss, C. A. & Fantner, E. J. (1993). *Mater. Sci. Forum*, **133–136**, 287–292.

Gier, T. E., Shannon, R. D. & Sonnichsen, G. C. (1986). US Patent 4 602 112.

Hill, R. J. & Howard, C. J. (1986). Report No. AAEC/M112. Australian Atomic Energy Commission (now ANSTO) Research Establishment, Lucas Heights, NSW, Australia.

Hovestreydt, E. (1983). *Acta Cryst.* A**39**, 268–269.

Kassner, D. (1993). *Reriet. A Program for Restrained Refinement of Powder Diffraction Data*. University of Frankfurt, Germany.

Keane, M. Jr, Sonnichsen, G. C., Abrams, L., Corbin, D. R., Gier, T. E. & Shannon, R. D. (1987). *Appl. Catal.* **32**, 361–366.

Koester, L. (1977). *Springer Tracts Mod. Phys.* **80**, 1–55.

Meier, W. M. & Kokotailo, G. T. (1965). *Z. Kristallogr.* **121**, 211–219.

Meier, W. M. & Villiger, H. (1969). *Z. Kristallogr.* **129**, 411–423.

Meyer, J. (1994). Phasencharakterisierung im ternären System Zeolith RHO–Trimethylamin–Wasser. Ph.D. thesis, Technische Hochschule Darmstadt, Germany.

Parise, J. B., Abrams, L., Gier, T. E., Corbin, D. R., Jorgensen, J. D. & Prince, E. (1984). *J. Phys. Chem.* **88**, 2303–2307.

Parise, J. B., Gier, T. E., Corbin, D. R. & Cox, D. E. (1984). *J. Phys. Chem.* **88**, 1635–1640.

Rietveld, H. M. (1969). *J. Appl. Cryst.* **2**, 65–71.

Robson, H. E., Shoemaker, D. P., Ogilvie, R. A. & Manor, P. C. (1973). In *Molecular Sieves*. Advances in Chemistry Series No. 121, edited by W. M. Meier & J. B. Uytterhoeven, pp. 106–115. Washington, DC: American Chemical Society.

Shannon, R. D., Staley, R. H., Vega, A. J., Fischer, R. X., Baur, W. H. & Auroux, A. (1989). *J. Phys. Chem.* **93**, 2019–2027.

Smith, J. V., Rinaldi, F. & Dent Glasser, L. S. (1963). *Acta Cryst.* **16**, 45–53.

Thomas, J. O. (1975). *Acta Cryst.* B**31**, 2156–2158.

Wiles, D. B. & Young, R. A. (1981). *J. Appl. Cryst.* **14**, 149–151.